ACS APPLIED MATERIALS & INTERFACES

www.acsami.org

Research Article

Machine Learning Enhanced Optical Microscopy for the Rapid Morphology Characterization of Silver Nanoparticles

Yaodong Xu, Da Xu, Ning Yu, Boqun Liang, Zhaoxi Yang, M. Salman Asif, Ruoxue Yan, and Ming Liu*

Cite This: *ACS Appl. Mater. Interfaces* 2023, 15, 18244−18251

Read Online

ACCESS | Metrics & More | Article Recommendations | Supporting Information

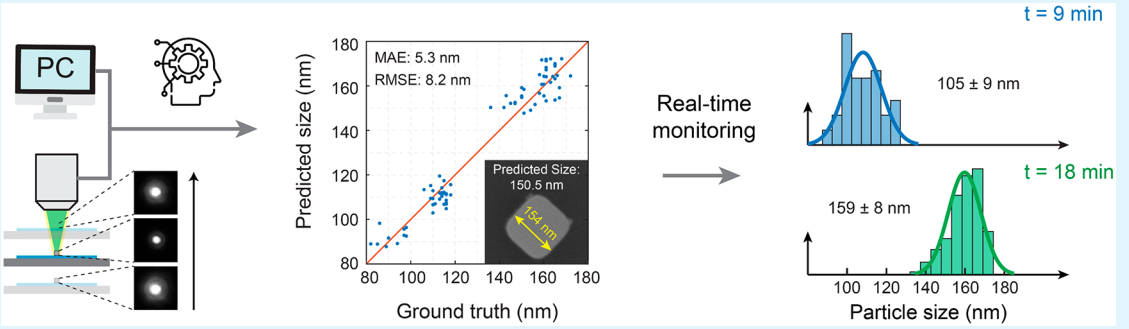

ABSTRACT: The rapid characterization of nanoparticles for morphological information such as size and shape is essential for material synthesis as they are the determining factors for the optical, mechanical, and chemical properties and related applications. In this paper, we report a computational imaging platform to characterize nanoparticle size and morphology under conventional optical microscopy. We established a machine learning model based on a series of images acquired by through-focus scanning optical microscopy (TSOM) on a conventional optical microscope. This model predicts the size of silver nanocubes with an estimation error below 5% on individual particles. At the ensemble level, the estimation error is 1.6% for the averaged size and 0.4 nm for the standard deviation. The method can also identify the tip morphology of silver nanowires from the mix of sharp-tip and blunt-tip samples at an accuracy of 82%. Furthermore, we demonstrated online monitoring for the evolution of the size distribution of nanoparticles during synthesis. This method can be potentially extended to more complicated nanomaterials such as anisotropic and dielectric nanoparticles.

KEYWORDS: *machine learning, convolutional neural network, through-focus optical microscopy, metal nanoparticles, particle size analysis, superimaging*

INTRODUCTION

Controlling the size and shape of nanoparticles is crucial for synthesizing nanomaterials due to their impact on the optical, chemical, and physicochemical properties of these materials. Specifically, nanoparticle size and shape affect essential properties such as the optical resonant frequency of plasmonics,[1−3] the catalytic activities of catalysts,[4−6] and the physicochemical efficacy of nanoparticle-based pharmaceutical products.[7] Significant scientific efforts have been devoted to developing new protocols to enrich the family of monodispersed nanoparticles with both isotropic and anisotropic geometries.[8,9] These efforts rely heavily on high-throughput size-characterization methods for monitoring particle morphology evolution, product quality control, and reaction mechanism study. Conventional nanoscale characterization techniques, such as electron microscopies (e.g., SEM and TEM) and dynamic light scattering (DLS),[10] either are time-consuming and cost-intensive or have a biased response on polydispersed samples as well as ligand-capped and anisotropic particles,[11,12] which have limited their applicability and spurred the need for alternative techniques. On the other hand, although optical microscopes are a popular low-cost and convenient characterization tool in research and industrial laboratories, their spatial resolutions are limited to approximately half of the illumination wavelength,[13] making them unsuitable for accurate size characterization of nanoparticles. As a result, there is a need for new approaches to improve nanomaterial characterization methods.

Through-focus scanning optical microscopy (TSOM), first introduced by Attota et al. in 2008,[14] has been proven accurate and high-throughput to characterize fabricated nanostructures.[15−18] Unlike conventional optical microscopy, which

Received: February 20, 2023
Accepted: March 23, 2023
Published: April 3, 2023

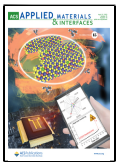

https://doi.org/10.1021/acsami.3c02448
ACS Appl. Mater. Interfaces 2023, 15, 18244−18251

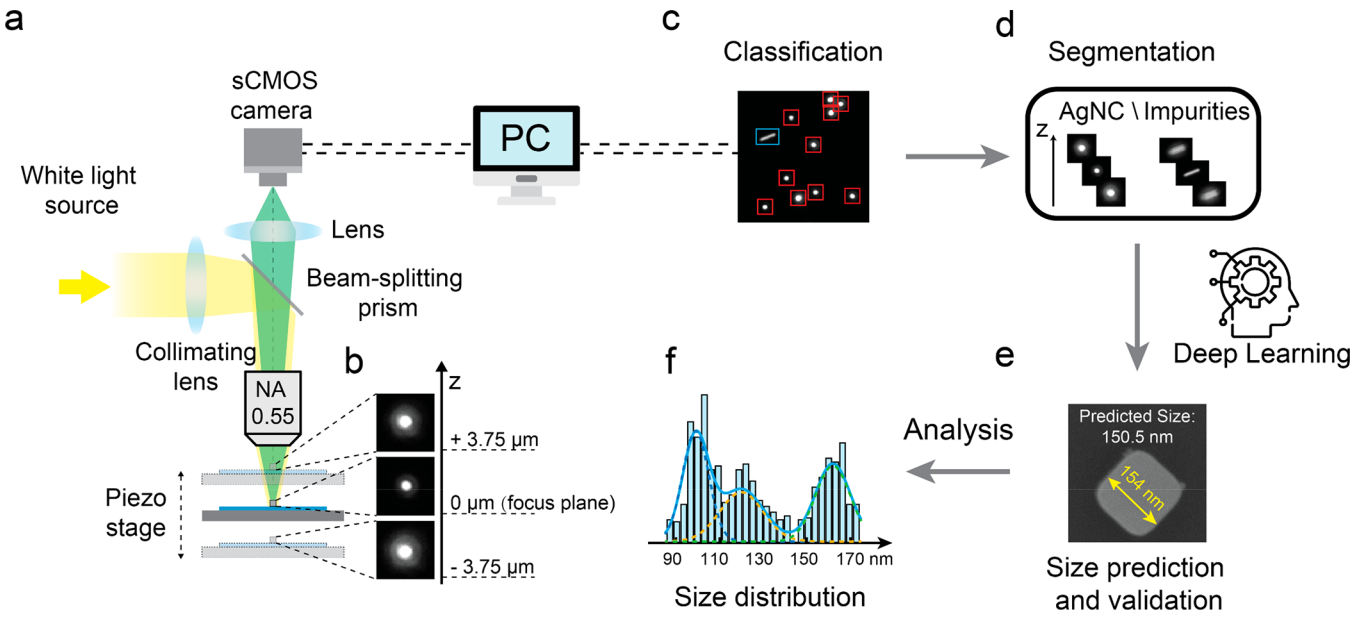

Figure 1. Schematic of the nanoparticle size prediction method incorporating the through-focus optical microscope imaging and the supervised machine learning. (a) The sample is swept across the focus plane by a piezo stage, generating a stacked image for data analysis. (b) Typical optical images of a nanoparticle at different focus/defocus positions. (c–e) Target classification, segmentation, and deep-CNN training. SEM-labeled data are used for the test. (f) Nanoparticle size and size distribution are acquired.

seeks to produce focused images with the sharpest contrast, TSOM captures a series of through-focus images with the focal plane sweeping through the sample object. These defocused images describe the evolution of light in the vicinity of the object, which is associated with the *k*-space distribution of the scattering light and, as predicted by the Mie theory,[19] is sensitive to the object size. The TSOM technique retrieves precise size information up to the subnanometer level by matching the through-focus images to a precalculated library with electromagnetic (EM) simulation results.[20,21] However, one limitation of TSOM is the few choices of sample geometries, primarily due to the expensive computation load required for a comprehensive library, which is aggravated if the EM simulations have the dimension expanded from 2D (e.g., nanowires or trenches) to 3D (e.g., nanoparticles) or include the variations in material optical properties for samples prepared with different fabrication methods. Data-driven machine learning algorithms can potentially remove the need for EM simulations and make TSOM an effective tool for predicting the size and morphology of nanomaterials from their diffraction-limited microscopy images.

In this paper, we describe a supervised machine learning algorithm, in combination with TSOM, for the precise analysis of nanomaterials, including size and morphology. The proposed algorithm achieves an estimation error of 5% at the single-particle level within a broad size range of 80–180 nm, while the error in the average size at the ensemble level is as low as 1.6%, with a size distribution error of merely 0.4 nm. To train the algorithm, a pseudo-labeling procedure was developed, which involves estimating particle size based on the percentile of the scattering intensity of a large number of nanoparticles with a known size distribution. In comparison with other particle-size analysis methods such ultraviolet–visible (UV–vis) absorption spectroscopy[22] and DLS,[23] the proposed machine learning assisted TSOM method allows for the estimation of individual particle size with high throughput and is capable of analyzing complex, polydispersed ensembles with broad size distributions. The performance of the proposed algorithm on other nanoscale features such as the tip morphology of nanowires is also evaluated. The approach has the potential to be widely applied to various types of nanomaterials and may facilitate the optimization of synthesis and processing strategies to achieve systematic and reproducible control over size tunability and dispersity.

RESULTS AND DISCUSSION

As illustrated in Figure 1a, the TSOM system is composed of an upright optical microscope, an sCMOS camera, and a piezoelectric positioner. A white light source with a color temperature of 3200 K was used for illumination, and a monochromatic camera was employed for imaging. The broad-bandwidth light source can smooth the spectral variation in the metal particle scattering spectrum, originating from the plasmonic resonant effect (refer to the Supporting Information for detailed information). To prepare samples for imaging, nanoparticles were deposited onto a SiO_2/Si wafer (300 nm SiO_2) using drop-casting followed by blow drying, creating a sparse layer of particles with a significant separation distance (5 to 10 μm between most particles) to avoid overlapping in the defocused images. The sample was mounted on the piezoelectric stage to capture TSOM stacked images. Each image stack consisted of 301 images with a 50 nm interval between focal planes and required approximately 30 s to acquire, with 50 to 100 nanoparticles included for subsequent data analysis. Lateral scanning of the sample was accomplished via a motorized microscope stage with a step size of approximately 100 μm, and the entire data acquisition process was completed in approximately 5 min. The collected data was sent to a computer for preprocessing.

The preprocessing procedure employed in this study to generate stacked optical images consists of two key steps: target prescreening and autofocusing. In the target prescreening step, a conventional computer vision approach is utilized to eliminate background noise from the CCD images and to

https://doi.org/10.1021/acsami.3c02448
ACS Appl. Mater. Interfaces 2023, 15, 18244–18251

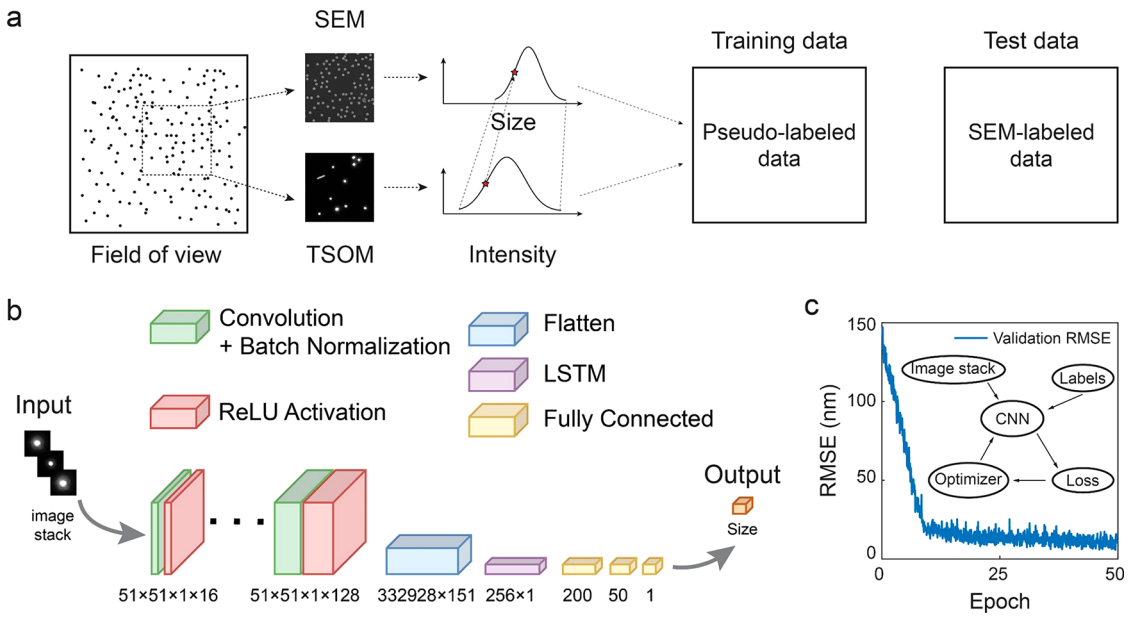

Figure 2. Machine learning data preparation, algorithm, and prediction accuracy. (a) The pseudolabeling step carries out the SEM characterization and TSOM measurements on different samples prepared from the same solution and generates the labels for the training data set based on their percentiles in the scattering intensity distribution. The test data set is prepared through a one-to-one comparison. (b) Workflow of the CNN, which is composed of 4, 4, 1, 1, and 3 layers for convolution, ReLU activation, flatten, LSTM, and fully connected layers, respectively. (c) The system RMSE in the training process.

discard images that contain impurities, such as nanowires, nanodisks, and large or small aggregates. While aggregates containing a few nanoparticles are typically unavoidable in colloidal samples, they are removed from the data set as their image profiles tend to be elliptical. Additional information about the prescreening algorithm is available in the Supporting Information. Following prescreening, stacked images containing individual nanoparticles are cropped from the original image and resized to 51 by 51 pixels. This size is sufficient to capture most of the optical evolution information. The 51-by-51 pixel size requires a minimum separation of approximately 5 μm between particles, and particles with a separation distance smaller than this requirement are discarded during preprocessing.

An autofocusing method is employed in this study to ensure that the on-focus images are placed at the center of each stack. This method involves segmenting the stacked images and identifying the on-focus image by evaluating the normalized variance of each image and selecting the one with the maximum value.[24,25] While this approach results in a reduction of the number of images per stack from 301 to 151, it ensures that the images used for training and testing are of the highest quality. Following the prescreening and autofocusing processes, the cropped stacks are combined with the labels and fed into a convolutional neural network (CNN) for further processing and analysis (see Figure 1e). The predicted sizes of a large quantity of particles can then be used to generate a statistical distribution of the nanoparticles (see Figure 1f).

The labels in the training data set were generated through an optical intensity-correlated pseudo-labeling method, which skips the one-to-one comparison between electron microscopy and optical microscopy images. This method is based on the fact that the statistical size distribution of nanoparticles is the same for both the TSOM measurement and the electron microscopy characterization. Although in practice the acquired size distributions may not be identical due to inaccuracies in statistical measures, their difference can be minimized by accumulating more data. To this end, we performed a large number of scanning electron microscopy (SEM) measurements (~1500 particles) to obtain accurate size distributions for six silver nanocube (AgNC) ensembles. An equivalent number of AgNCs were examined using TSOM, resulting in an intensity distribution based on optical scattering intensity. This distribution was then mapped to the size distribution obtained from SEM measurements to determine the size of each AgNC using its percentile in the intensity distribution. Such mapping between two distributions requires a linear relationship between the scattering intensity and the particle size, which has been confirmed through full-wave EM simulations (details in the Supporting Information). By eliminating the need for one-to-one comparison between the electron microscope results and the optical microscopy images, this pseudo-labeling method reduces the working load and saves a substantial amount of time, reducing the training-data preparation time from tens of hours to less than an hour. Notably, the size information from electron microscopy measurements is from random AgNCs, which do not necessarily need to be the same ones in the TSOM measurement.

In Figure 2b, we present the training workflow and network architecture, which utilizes a series of cropped image stacks comprising both pseudo-labeled and SEM-labeled sizes as inputs for training. The number of SEM-labeled data used in each training iteration was modified to evaluate the confidence of the pseudo-labeled data set. In the visible range, the scattering intensity of an AgNC is related to its diameter and microscope lamp power, which is susceptible to several fluctuating properties such as filament temperature, lamp voltage, and aging. To mitigate systematic error arising from intensity fluctuation, the stacked images were normalized sample-wise to the range of [0, 1], completely discarding the brightness information. The network architecture consists of four convolution layers, each with an increasing number of

https://doi.org/10.1021/acsami.3c02448
ACS Appl. Mater. Interfaces 2023, 15, 18244−18251

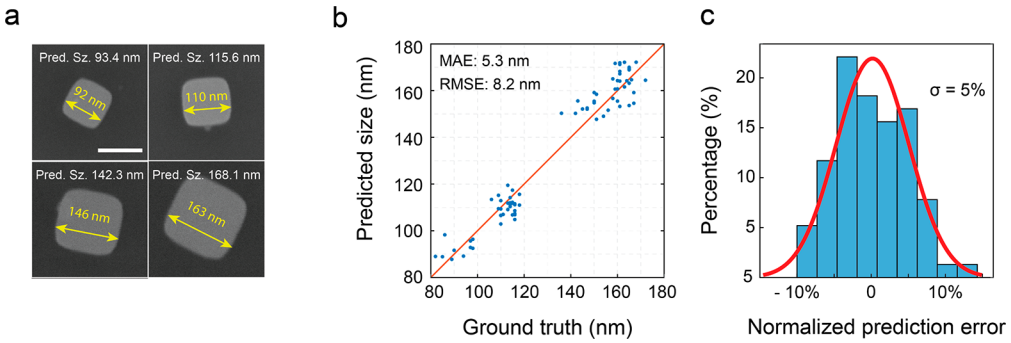

Figure 3. Performance evaluation of the CNN model. (a) SEM images of four AgNCs of different sizes, with the predicted and SEM-measured sizes labeled. The scale bar is 100 nm. (b) Correlation between the predicted and SEM-measured (ground truth) AgNC sizes. (c) Histogram of relative prediction errors and the Gaussian fit.

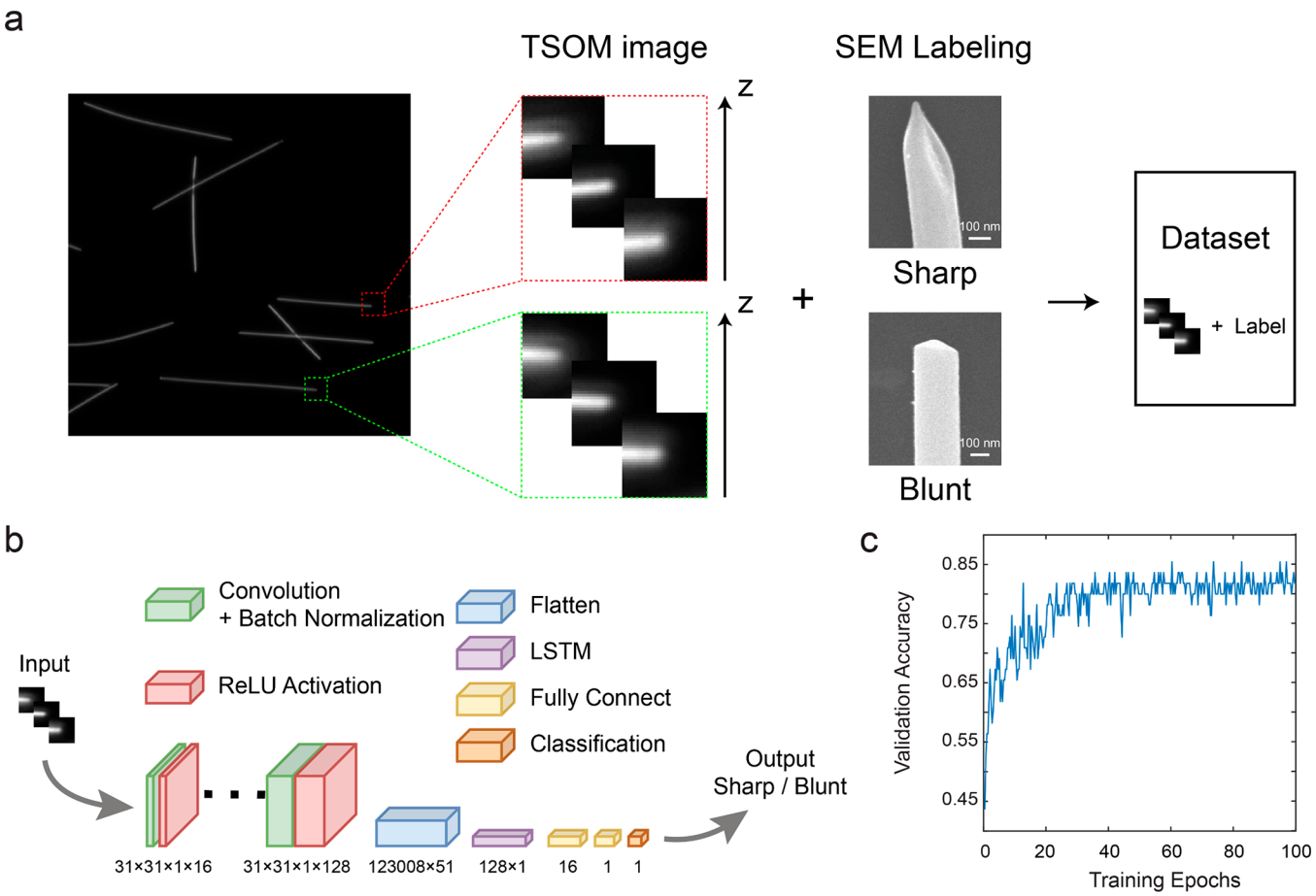

Figure 4. Classification of sharp and blunt tip AgNWs. (a) Generation of SEM-labeled AgNW tip classification data set. (b) Modified LST−CNN structure designed for AgNW tip classification, showing the reduced input dimension, a smaller LSTM layer, and a classification output layer. (c) Validation accuracy of the trained model, showing average accuracy of 81.82% after 100 epochs.

kernels to progressively extract features from the stacked images, followed by a batch normalization layer and a rectified linear unit (ReLU) activation layer. After feature extraction, the trained parameters are flattened and sent through long−short-term memory (LSTM) recurrent layers[26,27] to capture the evolution of scattered light in the stack, followed by a series of fully connected layers (typically three layers) to produce the final regression results, which are the predicted particle sizes in the model. To assess confidence of pseudolabeled data, we varied the portion of SEM-labeled data in the training set from 5% to 30% while keeping the size of the training data set fixed (550 pieces of stacked images) and observed that the use of pseudo-labeled data did not compromise the model performance. We present the root-mean-square error (RMSE) of a typical training process in Figure 2b, where RMSE reflects the accuracy of the trained CNN and has the unit of nanometer. Most trainings resulted in an RMSE of approximately 8 nm. To evaluate the role of the LSTM layer in the model, we trained a control group of networks that replaced the LSTM layer with either another fully connected layer or a global pooling layer. The performance of the control group (RMSE ∼ 18 nm) was significantly hindered compared to that of the LSTM−CNN

https://doi.org/10.1021/acsami.3c02448
ACS Appl. Mater. Interfaces 2023, 15, 18244−18251

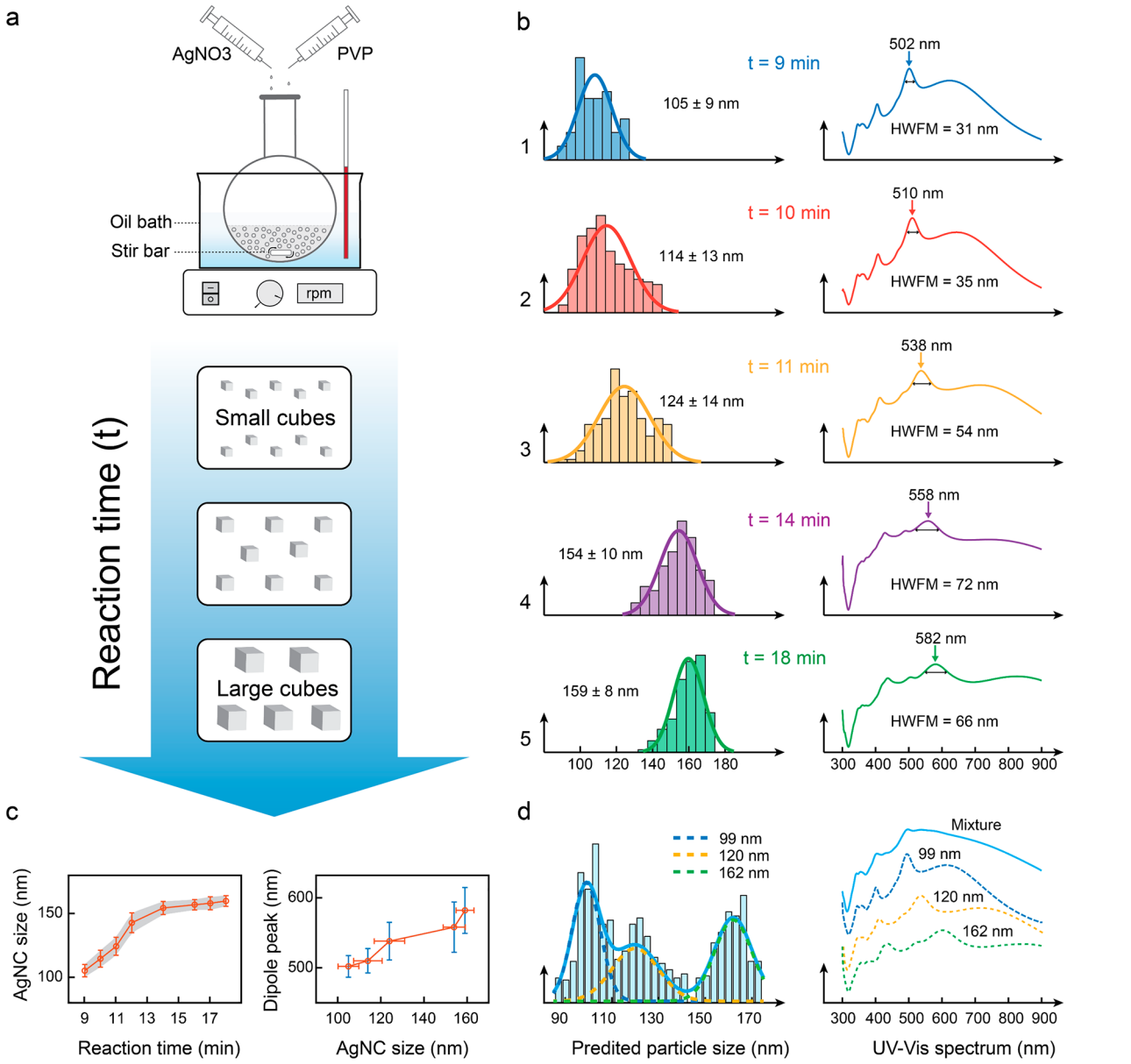

Figure 5. Evolution of the AgNC size distribution in a synthesis reaction. (a) Schematic illustration of the synthesis. (b) Five representative size distributions taken at different times after the reaction started, generated by the ML-assisted TSOM measurement (left column). The corresponding UV−vis absorption spectra are listed in the right column. (c) Left: size evolution over the reaction time. The error bars indicate the size deviation. Right: the wavelength of the selected plasmonic resonance peak (indicated by arrows in (b)) as a function of the predicted AgNC size. Error bars indicate the FWHM of the peak and the size deviation. (d) Size distribution of a mixture of AgNC with three different sizes acquired by the ML-assisted TSOM method (left) and the corresponding UV−vis absorption spectra (right).

model, as the former lacked the ability to capture the evolution of scattered light in the input data. A detailed comparison of the results is available in the Supporting Information.

As a proof-of-principle demonstration, we present the use of a CNN trained with only pseudo-labeled data to predict the size of AgNCs. Figure 3a displays SEM images of four representative AgNCs with different sizes and their predicted sizes labeled on the side. To further validate the performance of the model, an additional 78 AgNCs from three ensembles were examined, and their predicted sizes were compared with their actual sizes (ground truth) obtained from SEM images (resolution ~1.5 nm) in Figure 3b. A solid red line represents the perfect matching, and deviations from this line indicate the divergence between the predicted and true values. The model achieved a mean absolute error (MAE) of 5.3 nm and a root-mean-square error (RMSE) of 8.2 nm. The relative error normalized by the particle size is depicted in Figure 3c, which follows a Gaussian distribution with a standard deviation of 5% at the single particle level. At the statistical level, the mean errors of the sizes and size distributions for the three ensembles are 1.6% and 0.4 nm, respectively.

Following the validation of its capability in determining particle size, we investigated the algorithm's performance for quantifying the shapes of nanomaterials. Specifically, we utilized silver nanowires (AgNW) with distinct tip morphologies prepared via the modified polyol-mediated synthesis method described in our previous works.[28] The AgNW samples consisted of both sharp-tip and blunt-tip AgNWs, as

https://doi.org/10.1021/acsami.3c02448
ACS Appl. Mater. Interfaces 2023, 15, 18244−18251

shown by the SEM images in Figure 4a, where the sharp-tip AgNWs are particularly useful for near-field optical imaging.[29−31] Due to their small feature sizes, the AgNWs have tips and diameters beyond the diffraction limit and therefore are indistinguishable under conventional microscopy, as depicted by the optical microscopy images in Figure 4a. The CNN training workflow is illustrated in Figure 4b. The data set comprised 80 sharp-tip and 80 blunt-tip AgNWs drop-cast on a silicon wafer and verified with SEM imaging. To minimize the influence of optical aberrations from the microscope, all AgNWs were aligned in the same direction through the grazing-incidence-spraying drop-casting deposition.[32] Each TSOM image stack contained 51 images (31 by 31 pixels), as presented in the network structure schematic in Figure 4b. The 160 stacked images were randomly split into training (∼70% of the images) and validation (∼30%) data sets. As shown in Figure 4c, an average accuracy of 82% was achieved after training for 100 epochs. These results demonstrate the potential of our CNN-based approach for quantifying the shape of nanomaterials, with implications for a range of scientific and industrial applications.

Particle Size Evolution in Chemical Synthesis. The real-time monitoring of particle size evolution during nanomaterial synthesis is essential to address the challenges associated with systematic and predictable control over yield, size tunability, dispersity, and batch-to-batch reproducibility.[33−35] It can also accelerate parameter optimization and growth mechanism study[36] in a low-cost and time-effective way. Here, we tracked the particle size evolution over a 20 min synthesis of AgNC using a modified polyol synthesis approach.[37] Shortly after the start of the formation of faceted nanocubes, small aliquots (500 μL) were withdrawn from the reacting mixture every minute. The removal of an aliquot from the hot reaction mixture quenched nanoparticle growth in the aliquot due to a rapid drop in temperature, providing a snapshot of the nanoparticles in the continuing reaction. Each aliquot was divided into two parts. One part of each aliquot was drop-casted onto a substrate for TSOM inspection, while the other was diluted in ethanol for UV−vis measurement. UV−vis extinction spectroscopy combined with analytical frameworks such as Mie theory has been widely used as a convenient way for particle size analysis.[38] Figure 5b shows the CNN-predicted size distributions based on analyzing ∼300 nanoparticles from each sample and the corresponding UV−vis absorption spectra from the corresponding solutions. As shown in Figure 5c, a relatively linear growth rate of around 10 nm/min was observed at the early stage of the growth (t < 13 min), after which the growth slows to ∼2 nm/min as the growth of larger AgNCs was limited by the precursor feeding rate. The particle size distribution unambiguously narrowed down during this period, implying that this phase is important for the high-uniformity AgNCs. The UV−vis absorption spectra exhibit a red-shift in the plasmonic resonant wavelengths with the increase of AgNC size. Among the several plasmonic resonant features, the narrow peak with the second longest wavelength in the 500−600 nm range stems from the electric dipole oscillation with charges accumulated at the AgNC[39] and has been widely adopted to determine the AgNC size. Figure 5c confirms the relative linear relation between plasmonic resonance wavelength and particle size. Empirically, the peak width was also used to evaluate the size distribution qualitatively. However, this experience has strict limitations as the peak width was also limited by other factors, such as the sharpness of the nanocube edge and the shape dispersity of the sample. As shown in Figure 5c, the peak width (indicated by the vertical error bar) monolithically increases with the increase of AgNC size, although the width of the particle size distribution (the horizontal error bar) decreases.

The trained CNN has the potential to provide an effective solution for the analysis of complex nanoparticle systems that exhibit broad size distributions, which are typically unsuitable for analysis via UV−vis spectroscopy due to overlapping optical features. To demonstrate this capability, we conducted an experiment involving the mixing of three sample solutions, each with an average particle size of 99, 120, and 162 nm. The results obtained from the machine learning algorithm were compared with those obtained from UV−vis analysis. As depicted in Figure 5c, the CNN successfully identified the centers of the three particle sizes in the size distribution of 750 nanoparticles. However, the corresponding UV−vis spectrum exhibited a smearing of plasmonic features in the mixed solution, which rendered it unsuitable for accurate particle size prediction.

CONCLUSION

We present a machine learning algorithm that utilizes TSOM images to determine the size, size distribution, and shape of nanoparticles. To establish a training data set, we developed a pseudo-labeling method that avoids the time-consuming task of cross-referencing electron microscopy and optical microscopy images on a one-to-one basis. This algorithm reduces the preparation time for the training data set to less than an hour and the acquisition time for testing data to a few minutes. On AgNC samples, we achieved a single-particle level relative error of 5% and an ensemble-level averaged error of 1.6%. The algorithm can also classify the nanoscale tip geometry of AgNWs with an accuracy of 82%. We applied the machine learning algorithm to monitor the particle size evolution in a AgNC synthesis reaction and compared the results with those obtained from UV−vis analysis. The algorithm accurately visualizes particle size distribution, even for complex samples such as a mixture with a broad size distribution. We anticipate that this method can be expanded to examine complex nanoparticles with asymmetrical shapes, which introduce spatial variation along the azimuthal direction in the stacked TFM images that can be identified through machine learning. This technique requires only a conventional optical microscope and a motorized stage, enabling high-throughput size determination at the single-particle level, which has the potential to increase research productivity in the field of nanomaterials.

METHODS

Chemical Synthesis. The AgNCs were synthesized using a modified polyol method.[37] $AgNO_3$ (0.20 g) and $CuCl_2$ (0.34 ug) were dissolved in 10 mL of 1,5-pentanediol. In a separate vial, PVP (M_w = 55000 amu, 0.20 g) was dissolved in 10 mL of 1,5-pentanediol. After heating 20 mL of 1,5-pentanediol in a silicone oil bath (180 °C) for 10 min, two precursor solutions were dropwise added into the flask using two syringe pumps with a feeding rate of 500 μL/min. At various times during the whole synthesis, AgNC samples (500 μL) are extracted from the solution and divided equally into two portions for size analysis and UV−vis spectroscopy.

Optical Measurement. The home-built TSOM system comprises an upright optical microscope (Nikon, Eclipse Ni-U), a piezoelectric stage (P-545.3R8S PInano XYZ Piezo System), and a sCMOS camera (Andor, Zyla 4.2, 16 bit). A 50× dark-field objective lens with a

https://doi.org/10.1021/acsami.3c02448
ACS Appl. Mater. Interfaces 2023, 15, 18244−18251

Table 1. Monodisperse Silver Nanocubes Characterized by SEM

	sample 1	sample 2	sample 3	sample 4	sample 5	sample 6
mean size (nm)	90.30	116.63	138.50	154.84	164.94	178.07
STD (nm)	8.19	9.79	7.38	8.20	4.32	9.87
PDI	0.0082	0.0070	0.0028	0.0028	0.0007	0.0031

numerical aperture (NA) of 0.55 was used to illuminate the sample with white light and image the sample in the dark-field mode. The microscope system has a magnification scale of 125 nm/pixel. The sample was moved by the piezo stage at full speed and dwelled for 100 ms for every 50 nm displacement. The camera exposure time is 70 ms, with an extra 30 ms of waiting time. To generate a stacked image, a total of 301 images were acquired, taking 30 s for data acquisition. After classification and segmentation, the stacked image provided 50−100 nanoparticles for machine learning analysis.

Pseudo-labeling Method. The nanoparticle sizes were determined using scanning electron microscopy (SEM) imaging (ThermalFisher Scientific, model Nova NanoSEM 450), operating at 15 kV acceleration voltage and with a spatial resolution of 1.5 nm. The nanoparticles were deposited onto a silicon wafer using either Langmuir−Blodgett (LB) densely packed film[40] or drop-casting methods. The particle size information was extracted using ImageJ software. The training data set comprised six batches of AgNC samples with different sizes, and their mean particle sizes, standard deviation (STD), and polydispersity index (PDI) are presented in Table 1. The corresponding histograms of particle size distributions are available in the Supporting Information.

Training Configuration. The machine learning algorithm was realized through the deep learning toolbox on MATLAB. Model parameters are listed in Table 2.

Table 2. Training Configuration

training epochs	50	learn rate	1×10^{-4}
mini batch size	18	data shuffling	every epoch
optimizer	RMSprop	training hardware	GeForce RTX 2070

ASSOCIATED CONTENT

Supporting Information

The Supporting Information is available free of charge at https://pubs.acs.org/doi/10.1021/acsami.3c02448.

Optical scattering from AgNCs over the visible wavelength range; data set preparation from TSOM image stacks; representative TSOM images of AgNCs with different sizes; machine learning models for predicting AgNC particle size; influence from imaging quality; cross-validation for the pseudo-labeling method; comparison of different network structures (PDF)

AUTHOR INFORMATION

Corresponding Author

Ming Liu − *Materials Science and Engineering Program, University of California, Riverside, Riverside, California 92521, United States; Department of Electrical and Computer Engineering, University of California, Riverside, Riverside, California 92521, United States;* orcid.org/0000-0001-9849-1845; Email: ming@ece.ucr.edu

Authors

Yaodong Xu − *Materials Science and Engineering Program, University of California, Riverside, Riverside, California 92521, United States;* orcid.org/0000-0002-3859-9747

Da Xu − *Department of Electrical and Computer Engineering, University of California, Riverside, Riverside, California 92521, United States;* orcid.org/0000-0002-7554-426X

Ning Yu − *Chemical and Environmental Engineering, University of California, Riverside, Riverside, California 92521, United States*

Boqun Liang − *Materials Science and Engineering Program, University of California, Riverside, Riverside, California 92521, United States;* orcid.org/0000-0002-1163-2244

Zhaoxi Yang − *Chemical and Environmental Engineering, University of California, Riverside, Riverside, California 92521, United States*

M. Salman Asif − *Department of Electrical and Computer Engineering, University of California, Riverside, Riverside, California 92521, United States*

Ruoxue Yan − *Materials Science and Engineering Program and Chemical and Environmental Engineering, University of California, Riverside, Riverside, California 92521, United States;* orcid.org/0000-0002-0034-9806

Complete contact information is available at: https://pubs.acs.org/10.1021/acsami.3c02448

Author Contributions

Y.X. and D.X. contributed equally to this work.

Notes

The authors declare no competing financial interest.

ACKNOWLEDGMENTS

M.L. acknowledges support from the National Science Foundation (Nos. 1654746 and 1810453). R.Y. acknowledges support from the National Science Foundation (nos. 1654794 and 2022652).

REFERENCES

(1) Sherry, L. J.; Chang, S.-H.; Schatz, G. C.; Van Duyne, R. P.; Wiley, B. J.; Xia, Y. Localized Surface Plasmon Resonance Spectroscopy of Single Silver Nanocubes. *Nano Lett.* **2005**, *5* (10), 2034−2038.

(2) Yu, M.; Tian, Q.; He, G.; Cui, K.; Zhang, J. Surface-Enhanced Raman Scattering Fiber Probe Based on Silver Nanocubes. *Advanced Fiber Materials* **2021**, *3*, 349−358.

(3) Khurana, K.; Jaggi, N. Localized Surface Plasmonic Properties of Au and Ag Nanoparticles for Sensors: a Review. *Plasmonics* **2021**, *16* (4), 981−999.

(4) Gao, C.; Lyu, F.; Yin, Y. Encapsulated Metal Nanoparticles for Catalysis. *Chem. Rev.* **2021**, *121* (2), 834−881.

(5) Nguyen, L.; Tao, F. F.; Tang, Y.; Dou, J.; Bao, X.-J. Understanding Catalyst Surfaces during Catalysis through Near Ambient Pressure X-ray Photoelectron Spectroscopy. *Chem. Rev.* **2019**, *119* (12), 6822−6905.

(6) Wang, H.; Lu, J. A Review on Particle Size Effect in Metal-Catalyzed Heterogeneous Reactions. *Chin. J. Chem.* **2020**, *38* (11), 1422−1444.

(7) Takechi-Haraya, Y.; Ohgita, T.; Demizu, Y.; Saito, H.; Izutsu, K.-i.; Sakai-Kato, K. Current Status and Challenges of Analytical Methods for Evaluation of Size and Surface Modification of

Nanoparticle-Based Drug Formulations. *AAPS PharmSciTech* **2022**, *23* (5), 150.
(8) Dasgupta, N. P.; Sun, J.; Liu, C.; Brittman, S.; Andrews, S. C.; Lim, J.; Gao, H.; Yan, R.; Yang, P. 25th Anniversary Article: Semiconductor Nanowires − Synthesis, Characterization, and Applications. *Adv. Mater.* **2014**, *26* (14), 2137−2184.
(9) Zhao, Z.; Wang, X.; Jing, X.; Zhao, Y.; Lan, K.; Zhang, W.; Duan, L.; Guo, D.; Wang, C.; Peng, L.; et al. General Synthesis of Ultrafine Monodispersed Hybrid Nanoparticles from Highly Stable Monomicelles. *Adv. Mater.* **2021**, *33* (23), 2100820.
(10) Modena, M. M.; Rühle, B.; Burg, T. P.; Wuttke, S. Nanoparticle Characterization: What to Measure? *Adv. Mater.* **2019**, *31* (32), 1901556.
(11) Zheng, T.; Bott, S.; Huo, Q. Techniques for Accurate Sizing of Gold Nanoparticles Using Dynamic Light Scattering with Particular Application to Chemical and Biological Sensing Based on Aggregate Formation. *ACS Appl. Mater. Interfaces* **2016**, *8* (33), 21585−21594.
(12) Stetefeld, J.; McKenna, S. A.; Patel, T. R. Dynamic Light Scattering: a Practical Guide and Applications in Biomedical Sciences. *Biophysical Reviews* **2016**, *8* (4), 409−427.
(13) Mertz, J. *Introduction to Optical Microscopy.*; Cambridge University Press: 2019; p 43.
(14) Attota, R.; Silver, R.; Barnes, B. *Optical Through-Focus Technique that Differentiates Small Changes in Line Width, Line Height, and Sidewall Angle for CD, Overlay, and Defect Metrology Applications*; SPIE: 2008; Vol. *6922*.
(15) Attota, R. Through-Focus or Volumetric Type of Optical Imaging Methods: a Review. *Journal of Biomedical Optics* **2018**, *23* (7), 070901.
(16) Attota, R. K.; Kang, H. Parameter Optimization for Through-Focus Scanning Optical Microscopy. *Opt. Express* **2016**, *24* (13), 14915−14924.
(17) Park, S.-w.; Park, G.; Kim, Y.; Cho, J. H.; Lee, J.; Kim, H. Through-Focus Scanning Optical Microscopy with the Fourier Modal Method. *Opt. Express* **2018**, *26* (9), 11649−11657.
(18) Peng, R.; Qu, Y.; Hao, J.; Pan, H.; Niu, J.; Jiang, J. Multiple Parametric Nanoscale Measurements with High Sensitivity Based on Through-Focus Scanning Optical Microscopy. *J. Microsc.* **2019**, *274* (3), 139−149.
(19) Wang, H.; Brandl, D. W.; Nordlander, P.; Halas, N. J. Plasmonic Nanostructures: Artificial Molecules. *Acc. Chem. Res.* **2007**, *40* (1), 53−62.
(20) Attota, R.; Dixson, R. G. Resolving Three-Dimensional Shape of Sub-50 nm Wide Lines with Nanometer-Scale Sensitivity Using Conventional Optical Microscopes. *Appl. Phys. Lett.* **2014**, *105* (4), 043101.
(21) Attota, R.; Kavuri, P. P.; Kang, H.; Kasica, R.; Chen, L. Nanoparticle Size Determination Using Optical Microscopes. *Appl. Phys. Lett.* **2014**, *105* (16), 163105.
(22) Tan, E. X.; Chen, Y.; Lee, Y. H.; Leong, Y. X.; Leong, S. X.; Stanley, C. V.; Pun, C. S.; Ling, X. Y. Incorporating Plasmonic Featurization with Machine Learning to Achieve Accurate and Bidirectional Prediction of Nanoparticle Size and Size Distribution. *Nanoscale Horizons* **2022**, *7* (6), 626−633.
(23) Hussain, R.; Alican Noyan, M.; Woyessa, G.; Retamal Marín, R. R.; Antonio Martinez, P.; Mahdi, F. M.; Finazzi, V.; Hazlehurst, T. A.; Hunter, T. N.; Coll, T.; Stintz, M.; Muller, F.; Chalkias, G.; Pruneri, V. An Ultra-Compact Particle Size Analyser Using a CMOS Image Sensor and Machine Learning. *Light: Science & Applications* **2020**, *9* (1), 21.
(24) Sun, Y.; Duthaler, S.; Nelson, B. J. Autofocusing in Computer Microscopy: Selecting the Optimal Focus Algorithm. *Microscopy research and technique* **2004**, *65* (3), 139−149.
(25) Bian, Z.; Guo, C.; Jiang, S.; Zhu, J.; Wang, R.; Song, P.; Zhang, Z.; Hoshino, K.; Zheng, G. Autofocusing Technologies for Whole Slide Imaging and Automated Microscopy. *Journal of Biophotonics* **2020**, *13* (12), e202000227.
(26) Huang, S.; Jin, G.; Jiyun, M. Enhanced Magneto-optic Imaging Based on LSTM-CNN Model and Multi-modal Fusion, 2021 IEEE International Conference on Emergency Science and Information Technology (ICESIT), 22−24 Nov 2021; 2021; pp 612−621.
(27) Ritter, C.; Spilger, R.; Lee, J. Y.; Bartenschlager, R.; Rohr, K. Deep Learning For Particle Detection And Tracking In Fluorescence Microscopy Images, 2021 IEEE 18th International Symposium on Biomedical Imaging (ISBI), 13−16 April 2021; 2021; pp 873−876.
(28) Ma, X.; Zhu, Y.; Kim, S.; Liu, Q.; Byrley, P.; Wei, Y.; Zhang, J.; Jiang, K.; Fan, S.; Yan, R.; Liu, M. Sharp-Tip Silver Nanowires Mounted on Cantilevers for High-Aspect-Ratio High-Resolution Imaging. *Nano Lett.* **2016**, *16* (11), 6896−6902.
(29) Ma, X.; Liu, Q.; Yu, N.; Xu, D.; Kim, S.; Liu, Z.; Jiang, K.; Wong, B. M.; Yan, R.; Liu, M. 6 nm Super-Resolution Optical Transmission and Scattering Spectroscopic Imaging of Carbon Nanotubes Using a Nanometer-Scale White Light Source. *Nat. Commun.* **2021**, *12* (1), 6868.
(30) Ma, X.; Zhu, Y.; Yu, N.; Kim, S.; Liu, Q.; Apontti, L.; Xu, D.; Yan, R.; Liu, M. Toward High-Contrast Atomic Force Microscopy-Tip-Enhanced Raman Spectroscopy Imaging: Nanoantenna-Mediated Remote-Excitation on Sharp-Tip Silver Nanowire Probes. *Nano Lett.* **2019**, *19* (1), 100−107.
(31) Kim, S.; Yu, N.; Ma, X.; Zhu, Y.; Liu, Q.; Liu, M.; Yan, R. High External-Efficiency Nanofocusing for Lens-Free Near-Field Optical Nanoscopy. *Nat. Photonics* **2019**, *13* (9), 636−643.
(32) Hu, H.; Pauly, M.; Felix, O.; Decher, G. Spray-Assisted Alignment of Layer-by-Layer Assembled Silver Nanowires: a General Approach for the Preparation of Highly Anisotropic Nano-Composite Films. *Nanoscale* **2017**, *9* (3), 1307−1314.
(33) Roduner, E. Size Matters: Why Nanomaterials are Different. *Chem. Soc. Rev.* **2006**, *35* (7), 583−592.
(34) Tao, H.; Wu, T.; Aldeghi, M.; Wu, T. C.; Aspuru-Guzik, A.; Kumacheva, E. Nanoparticle Synthesis Assisted by Machine Learning. *Nat. Rev. Mater.* **2021**, *6* (8), 701−716.
(35) Njoki, P. N.; Luo, J.; Kamundi, M. M.; Lim, S.; Zhong, C.-J. Aggregative Growth in the Size-Controlled Growth of Monodispersed Gold Nanoparticles. *Langmuir* **2010**, *26* (16), 13622−13629.
(36) Park, K.; Drummy, L. F.; Wadams, R. C.; Koerner, H.; Nepal, D.; Fabris, L.; Vaia, R. A. Growth Mechanism of Gold Nanorods. *Chem. Mater.* **2013**, *25* (4), 555−563.
(37) Wiley, B.; Herricks, T.; Sun, Y.; Xia, Y. Polyol Synthesis of Silver Nanoparticles: Use of Chloride and Oxygen to Promote the Formation of Single-Crystal, Truncated Cubes and Tetrahedrons. *Nano Lett.* **2004**, *4* (9), 1733−1739.
(38) Panariello, L.; Radhakrishnan, A. N. P.; Papakonstantinou, I.; Parkin, I. P.; Gavriilidis, A. Particle Size Evolution during the Synthesis of Gold Nanoparticles Using In Situ Time-Resolved UV−Vis Spectroscopy: An Experimental and Theoretical Study Unravelling the Effect of Adsorbed Gold Precursor Species. *J. Phys. Chem. C* **2020**, *124* (50), 27662−27672.
(39) Hung, L.; Lee, S. Y.; McGovern, O.; Rabin, O.; Mayergoyz, I. Calculation and Measurement of Radiation Corrections for Plasmon Resonances in Nanoparticles. *Phys. Rev. B* **2013**, *88* (7), 075424.
(40) Tao, A.; Sinsermsuksakul, P.; Yang, P. Polyhedral Silver Nanocrystals with Distinct Scattering Signatures. *Angew. Chem., Int. Ed.* **2006**, *45* (28), 4597−4601.

https://doi.org/10.1021/acsami.3c02448
ACS Appl. Mater. Interfaces 2023, 15, 18244−18251